Journal of Coastal Research	SI	116	578-582	Charoltte, North Carolina	2023

Optimal Design of the Overtopping Wave Energy Converter Based on Fluid–Structure Interaction Simulation

Sung-Hwan An[†], Geun-Gon Kim[‡], and Jong-Hyun Lee[‡*]

[†]Department of Ocean System Engineering
Gyeongsang National University
Tongyeong, Republic of Korea

[‡]Department of Naval Architecture and Ocean Engineering
Gyeongsang National University
Tongyeong, Republic of Korea

www.cerf-jcr.org

www.JCRonline.org

ABSTRACT

An, S.-H.; Kim, G.-G., and Lee, J.-H., 2023. Optimal design of the overtopping wave energy converter based on fluid–structure interaction simulation. *In:* Lee, J.L.; Lee, H.; Min, B.I.; Chang, J.-I.; Cho, G.T.; Yoon, J.-S., and Lee, J. (eds.), *Multidisciplinary Approaches to Coastal and Marine Management*. *Journal of Coastal Research*, Special Issue No. 116, pp. 578-582. Charlotte (North Carolina), ISSN 0749-0208.

The wave overtopping system in wave power generation systems is called the Overtopping Wave Energy Converter (OWEC). The performance of the OWEC is affected by wave height and period. Wave characteristics, such as wave height, period, and direction, vary with environmental conditions, which make it difficult for the OWEC to generate stable electric power. To mitigate this issue, appropriate OWEC designs based on environmental conditions and wave characteristics must be investigated. In this study, the hydraulic efficiency of the OWEC and the load acting on it were calculated using the Smoothed Particle Hydrodynamics (SPH) based on the environmental conditions along the Ulleungdo coast, and the structural safety of the optimized OWEC model was verified. Moreover, a particle-based simulation was performed to confirm the effect of design parameters on energy efficiency. Additionally, the load acting on the OWEC was calculated, and the optimization method was used to design six types of substructures. Finally, structural analysis was conducted, confirming that all six types avoided the design model's structural resonance period.

ADDITIONAL INDEX WORDS: *Overtopping Wave Energy Converter, smoothed particle hydrodynamics, structural analysis, design optimization.*

INTRODUCTION

After the Paris Climate Agreement in 2016, major emitters set the goal of reducing greenhouse gas emissions by 25%–65% by 2030. Accordingly, they are using environmentally friendly renewable energy systems instead of carbon energy systems. The ocean energy system, which is a renewable energy system, has various potential energy sources. Given Korea's high proportion of coastline, it has great potential for generating energy from the ocean (*e.g.*, 6,500 MW from tidal and wave energy, 4,000 MW from ocean thermal energy conversion, and 1,000 MW from current energy). Additionally, for the ocean energy system compared to onshore energy system, securing a site for large-scale complex construction is more feasible, and there are fewer problems, such as noise and destruction of the natural environment.

Movable body-type wave energy converters, oscillating water columns-type wave energy converters and Overtopping Wave Energy Converter (OWEC) are types of wave power generators. The OWEC converts the kinetic energy of waves overtopping each reservoir into potential energy to rotate the turbine. Overtopping discharge in each reservoir affects its power generation. Accordingly, researchers have focused on the discharge based on the design of the OWEC. Kofoed (2005) measured the discharge in each reservoir according to the design of the wave power generator through model experiments. Liu, Hyun, and Jin (2009) proposed the optimal design by comparing the design of the OWEC ramp of the straight-line and parabolic types. Park, Shin, and Hong (2011) proposed an optimal operation method of the OWEC through a model experiment. Victor, Troch, and Kofoed (2011) compared and verified the efficiency of each wave power generator design via theoretical calculations. Jungrungruengtaworn and Hyun (2017) analyzed the energy efficiency according to the length of the slot of the multistage OWEC. Finally, Mustapa, Yaakob, and Ahmed (2019) proposed the slope design of the sea wave slot-cone generator based on 3D analysis results.

In this study, the substructure of the OWEC was designed, and numerical simulations were performed to calculate its energy efficiency and structural safety. DualSPhysics, based on a particle-based fluid analysis method, was used for fluid flow analysis, and Ansys, a structural analysis program, was used for structural analysis. Before designing the OWEC, the wave characteristics along the coast of Korea and Ulleungdo were studied (Kim, An, and Lee, 2022). Then, a simulation was conducted by changing the design of the OWEC substructure, and the optimal design was derived based on the simulation results.

DOI: 10.2112/JCR-SI116-117.1 received 6 March 2023; accepted in revision 21 April 2023.
*Corresponding author: gnujhlee@gnu.ac.kr

METHODS

This section explains the Smoothed Particle Hydrodynamics (SPH) and allowable stress used in the design, analysis, and simulation of the OWEC.

SPH Method Kernel Function

SPH is based on the Lagrangian method, which expresses fluid flows as particles. Each particle has physical quantities, such as mass, density, pressure, and velocity. The physical quantities of fluid particles are estimated by the integration of the weighting function as follows:

$$F(r) = \int F(r')W(r - r', h)dr, \tag{1}$$

where, $F(r)$ is the physical quantity at point r, r is an arbitrary position vector, and $W(r - r', h)$ is a kernel function using the smoothing length h and is defined as follows:

$$W(\boldsymbol{r}, h) = \alpha_D \begin{cases} 1 - \frac{2}{3}q^2 + \frac{3}{4}q^3 & 0 \le q < 1 \\ \frac{1}{4}(2-q)^3 & 1 \le q < 2 \\ 0 & q \ge 2 \end{cases} \tag{2}$$

where, $\boldsymbol{r}$ is the distance between two different particles $r - r'$. q is the dimensionless distance between particles in r/h. α_D is $10/7\pi h^2$ for two dimensions and $1/\pi h^3$ for three dimensions. Equation (1) is approximated in discretized form and is represented as follows:

$$F(r) = \sum_b F(r)\frac{m_b}{\rho_m}W(r - r_b, h), \tag{3}$$

where, b denotes an individual particle, m_b and ρ_m denote the mass and density of particle b, respectively.

Allowable Stress

The allowable stress condition (API-RP-2A-WSD) was used to evaluate the safety of the structure. The allowable stress condition is considered safe when the equivalent stress generated under the design load does not exceed the allowable stress of the member. In API-RP-2A-WSD, the function for calculating the allowable tensile and compressive stresses of steel pipe members is as follows:

$$F_t = 0.6F_y \tag{4}$$

$$F_a = \frac{\left[1 - \frac{(kl/r)^2}{2C_C^2}\right]F_y}{5/3 + \frac{3(kl/r)}{8C_C} - \frac{(kl/r)^3}{8C_C^2}} \tag{5}$$

where, F_t is the allowable tensile stress, F_y is the yield strength, F_a is the allowable compressive stress, $C_C = \left(\frac{2\pi^2 E}{F_y}\right)^{\frac{1}{2}}$, E is the modulus of elasticity, k is the effective length factor (1.0 for truss legs), and l and r are the distance between braces and the turning radius, respectively.

RESULTS

This section confirms the effects of substructure design on the energy efficiency of OWEC using SPH simulation. In addition, the wave load acting on the OWEC is measured and then applied to the design optimization process. The safety of the OWEC is determined through static structural analysis and dynamic characteristic analysis.

SPH Simulation

The environmental conditions analyzed by Kim, An, and Lee (2022) along the Ulleungdo coast were selected. The wave conditions used for analysis were 1/10 scale of the significant wave height calculated from 10-year return period and the maximum wave height calculated from 100-year return period. The significant wave height was used to calculate the wave energy, and the maximum wave height was used to calculate the load used in the structural safety analysis. The conditions of the waves are described in Table 1.

Table 1. *10-year and 100-year wave conditions of each scale.*

	10-year Significant Wave		100-year Maximum Wave	
	1/1 Scale	1/10 Scale	1/1 Scale	1/10 Scale
Wave Height [m]	2.8	0.28	4.24	0.424
Wave Period [s]	7.37	2.33	7.72	2.44

The standard model was designed based on those of An *et al.* (2022), Jungrungruengtaworn and Hyun (2017), Vicinanza *et al.* (2012), and Victor, Troch, and Kofoed (2011). To confirm the effect of the length factor, the bottom length of OWEC substructures was reduced at 6-m intervals as a design variable. The designed models are shown in Figure 1.

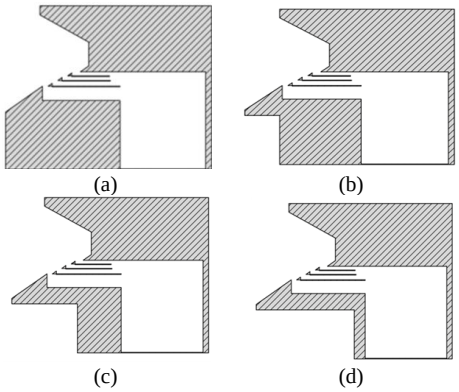

Figure 1. Designed models Standard (a), Model 1 (−6 m) (b), Model 2 (−12 m) (c), and Model 3 (−18 m) (d).

The 2D numerical wave tank used herein is shown in Figure 2. The distance between the piston-type wavemaker and the OWEC is 8 m, and the water depth is 1.8 m. The 3-m domain after the

OWEC was designated as a damping zone to reduce the effect of reflected waves.

The overall efficiency of the OWEC comprises four partial efficiencies (*i.e.*, hydraulic, reservoir, turbine, and generator efficiencies). Hydraulic efficiency, which represents the overtopping performance, was used in this study. It is defined as the proportion of hydraulic power P_{crest} to wave power P_{wave}:

$$\eta_{hydr} = \frac{P_{crest}}{P_{wave}}, \quad (6)$$

$$P_{crest} = \sum_{j=1}^{n} \rho g q_j R_{c,j}, \quad (7)$$

$$P_{wave} = \frac{1}{8}\rho g H^2 \mathrm{c} \frac{1}{2}\left[1 + \frac{2kd}{\sinh(kd)}\right], \quad (8)$$

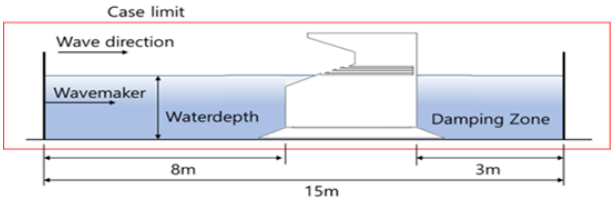

Figure 2. Geometry of 2-Dimensuional tank.

where, ρ is the density of the fluid, g is the gravitational acceleration, c is the wave phase velocity, k is the wave number, q_j is the average discharge of the j^{th} reservoir, and $R_{c,j}$ is the crest height of the j^{th} reservoir.

The simulation results in Table 2 show that the hydraulic efficiency decreases with the substructure length but does not affect the performance of the OWEC. In the case of Model 3, a substructure must be designed to support the OWEC superstructure. Therefore, to calculate the load on the wave acting on the OWEC, simulation was performed under the maximum wave height determined from 100-year return period. The loads on the ramp and vertical wall of the ramp were measured; the results are shown in Table 3.

Table 2. *Hydraulic efficiency of each models.*

	$\eta_{hydr,1}$	$\eta_{hydr,2}$	$\eta_{hydr,3}$	$\eta_{hydr,4}$	$\eta_{hydr,all}$
Original	0.107	0.158	0.080	0.023	0.367
Mdoel_1	0.107	0.160	0.090	0.010	0.367
Model_2	0.112	0.158	0.083	0.009	0.362
Model_3	0.114	0.161	0.076	0.009	0.360

Table 3. *Force acting on the Ramp and Vertical wall.*

Axis	Slope of Ramp [N]	Vertical wall [N]
X	1270	917.51
Y	0	0
Z	-2510	-291.84

Optimization of OWEC Models

The design of the OWEC substructures was optimized using Altair's Inspire program to reduce their weight. The design loads listed in Table 2 were applied to the structural model, and the 3D model substructure design was optimized by adjusting the volume ratio of the design area. Thus, the weight of the standard model could be reduced by 30%–50% (Figure 3); simultaneously, a deformed truss structure that could effectively distribute the self-weight and environmental load was derived.

Structural analysis was performed to verify the structural safety of the optimized model. A substructure composed of line elements was also modeled for analyzing the truss structures. They were designed with the diameter and thickness of the leg and brace according to the volume ratio. Model parameters for each case are shown in Table 4, where D_L is the diameter of the main leg of the substructure, D_B is the diameter of the brace of the substructure, and t_L and t_B are the thicknesses of the main leg and brace, respectively.

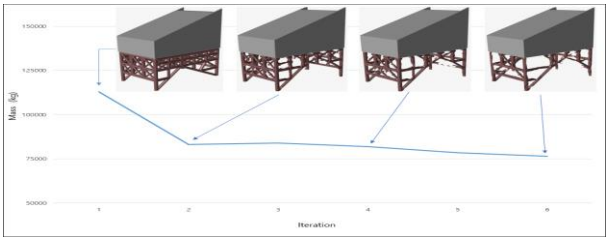

Figure 3. Design optimization results by iteration.

Table 4. *Considered scenarios with respect to parameters of the members.*

	Volume [%]	D_L [mm]	D_B [mm]	t_L [mm]	t_B [mm]
Case 1	50				
Case 2	40	1000	500	25	10
Case 3	30				
Case 4	50				
Case 5	40	300	150	50	20
Case 6	30				

Load Conditions

Types of loads acting on structures based on API-RP-2A-WSD include wave, current, wind, sea ice, and hydrostatic loads. In this study, the wave, current, and hydrostatic loads were applied as environmental loads on the substructures; the results are shown in Table 5.

Table 5. *Loads applied to the substructure.*

Load		Value
1. Static Load		32.1E+6 [N]
2. Hydrostatic load	7 [m]	2.1E+5 [N]
	9 [m]	2.7E+5 [N]
	11 [m]	3.3E+5 [N]
	13 [m]	3.9E+5 [N]
	15 [m]	4.5E+5 [N]
3. Current Load		884.8 [N/m]
4. Wave Load		1,780 [N/m]

Structural Analysis

Static structural analysis was performed to verify the accuracy of the optimization results. The boundary and load conditions used for the structural analysis are shown in Figure 4. As a boundary condition, all translational and rotational degrees of

freedom of the support point of the leg were constrained considering the foundation pile fixation of the structure. Additionally, the self-weight of the superstructure was given in the z direction. The wave and current loads were summed for each direction component and then assigned to the x direction, which is the wave direction. The hydrostatic loads for each depth were calculated and applied at each point of the substructure.

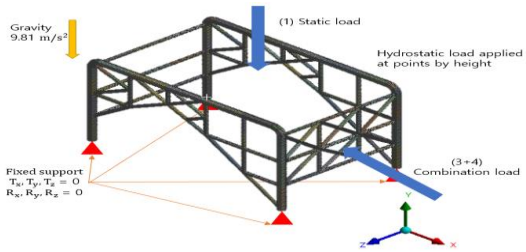

Figure 4 Boundary and loading conditions imposed on the substructure model.

Dynamic Characteristic Analysis

Modal and harmonic response analyses were performed as dynamic characteristic analysis methods for the OWEC substructure. Modal analysis was performed to calculate the natural frequency of the OWEC substructure and to confirm the dynamic effects of environmental loads.

In the harmonic response analysis, after confirming the mode shape of the OWEC substructure, the corresponding frequency was designated as the region of interest. For the steady load condition, the fluid particle acceleration was calculated based on the significant wave height and wave period of the 1-year return period of Ulleungdo coast and applied as the excitation force of the harmonic response analysis. A damping ratio of 5% was applied because a damping effect of 3%–5% is considered in a general mechanical system.

DISCUSSION

The results of the analysis of the axial tensile and compressive stresses are shown in Table 5. The dominant load of the vertical stress generated in the main member was identified as the weight of the superstructure. A tensile stress of approximately 41.3 MPa occurred in the upper leg. The maximum compressive stress was generated in the truss leg by the weight of the superstructure. For each case where the volume ratio was reduced, the compressive stress tended to increase but did not exceed the allowable compressive stress. For Cases 1, 3, and 4 in Table 6, tensile stress exceeding 41.3 MPa occurred at the end of the connecting member. In all cases, the allowable tensile and compressive stresses suggested by API-RP-2A-WSD did not exceed the allowable limit.

Table 6 *Structural safety assessment result (unit: MPa).*

Case	$\sigma_{tension}$	σ_{comp}	Ft	Fa	Remark
Case 1	55	56	150	147	O.K.
Case 2	41	57			O.K.
Case 3	96.9	64			O.K.
Case 4	87	96.9			O.K.
Case 5	41	97			O.K.
Case 6	45	106			O.K.

Modal analysis was performed for two cases: the initial model before weight reduction and the optimal model (Case 6). The natural frequency tendency of the substructure was measured (Table 7). The natural frequency of the designed structure did not correspond to the wave period of the wave data measured for 10 years in Ulleungdo coast, confirming that the substructure was designed to avoid the resonance period.

Table 7 *Modal analysis result (unit: Hz).*

Model Type	Mode	Natural frequency
Initial Model	1st mode	1.3
	2nd mode	2.78
	3rd mode	8.1
Case 6	1st mode	0.99
	2nd mode	1.37
	3rd mode	7.77

The harmonic response analysis results confirmed that the most significant response occurred at a frequency of 2.784 Hz for the initial model. The maximum acceleration was 6435.6 mm/s^2, and the maximum response occurred at the phase angle of −92.833°. On the other hand, for the optimized model, the most significant response occurred at a frequency of 1.37 Hz. The maximum acceleration was 3175.4 mm/s^2, and the maximum response occurred at −92.771°, similar to the phase angle of the initial model. The response of the optimal model was significantly reduced compared with that of the initial model (Figure 5).

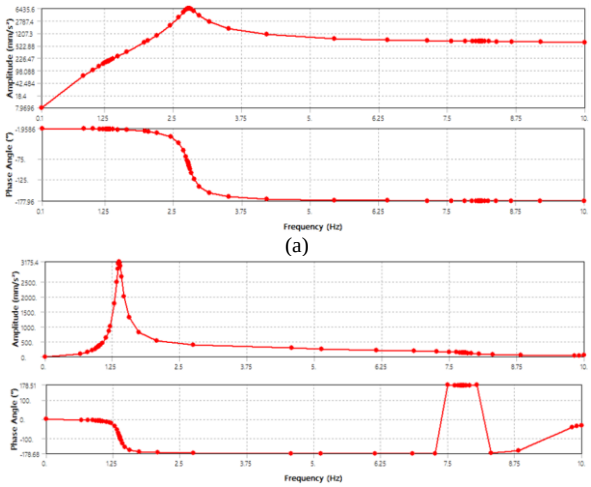

(a)

(b)

Figure 5 Harmonic response analysis results Initial model (a) and Case 6 (b).

CONCLUSIONS

Herein, a computer simulation was performed to determine the energy efficiency and structural safety of OWEC substructures. Based on the wave characteristics and environmental conditions in Ulleungdo coast, a particle-based simulation was conducted to confirm their effect on energy efficiency and the load acting on the OWEC. Subsequently, the OWEC substructure design was optimized based on the calculated load. The structural safety of the designed models was confirmed through static structural

analysis and dynamic characteristic analysis. Results confirmed that the optimal design model was designed to avoid the frequency period of Ulleungdo coast. However, the diversity of design variables requires improvement, and the reliability of simulation results needs to be secured. The application of various design variables and the reliability of simulation results must be studied through model tests.

ACKNOWLEDGMENTS

This work was supported by National R&D Program through the National Research Foundation of Korea (NRF) funded by the Korea government (Ministry of Science and ICT) (No. 2021R1I1A3057230).

LITERATURE CITED

An, S.H.; Kim, G.G., and Lee, J.H., 2022. The effect of hydraulic efficiency on the design variables of an overtopping wave energy converter. *Journal of the Korean Society of Marine Environment & Safety*, 28(1), 168-174.

Jungrungruengtaworn, S. and Hyun, B.S., 2017. Effects of structure geometry on energy harvesting efficiency of multi-stage overtopping wave energy converters. *Journal of the Korean Society for Marine Environment & Energy*, 20(3), 136-144.

Kim, G.G.; An, S.H., and Lee, J.H., 2022. Review of the optimal locations of coastal sea area for operating wave energy converter in Korea. *Journal of Advanced Marine Engineering and Technology*, 46(4), 172-181.

Kofoed, J.P., 2005. Model testing of the wave energy converter seawave slot-cone generator. *Hydraulics and Coastal Engineering*, 18, 31.

Liu, Z.; Hyun, B.S., and Jin, J.Y., 2009. Computational analysis of parabolic overtopping wave energy convertor. *Journal of the Korean Society for Marine Environment & Energy*, 12(4), 273-278.

Mustapa, M.A.; Yaakob, O.B., and Ahmed, Y.M., 2019. Numerical simulation of the overtopping-ramp design of a multistage overtopping wave energy breakwater hybrid device. *International Journal of Innovative Technology and Exploring Engineering*, 8(12), 5531-5538.

Park, J.Y.; Shin, S.H., and Hong, K.Y., 2011. Experimental study for overtopping performance and control system of overtopping wave energy convertor. *Journal of the Korean Society for Marine Environment & Energy*, 14(1), 11-18.

Vicinanza, D.; Margheritini, L.; Kofoed, J.P., and Buccino, M., 2012. The SSG wave energy converter: Performance, status and recent developments. *Energies*, 5(2), 193-226.

Victor, L., Troch, P., and Kofoed, J.P., 2011. On the effects of geometry control on the performance of overtopping wave energy converters. *Energies*, 4(10), 1574-1600.